

# Evaluation of a $^{64}\text{Cu}$ -Labeled Cystine-Knot Peptide Based on Agouti-Related Protein for PET of Tumors Expressing $\alpha_v\beta_3$ Integrin

Lei Jiang<sup>\*1,2</sup>, Richard H. Kimura<sup>\*2</sup>, Zheng Miao<sup>2</sup>, Adam P. Silverman<sup>3</sup>, Gang Ren<sup>2</sup>, Hongguang Liu<sup>2</sup>, Peiyong Li<sup>1</sup>, Sanjiv Sam Gambhir<sup>2,3</sup>, Jennifer R. Cochran<sup>3</sup>, and Zhen Cheng<sup>2</sup>

<sup>1</sup>Department of Nuclear Medicine, Ruijin Hospital, Shanghai Jiaotong University, Shanghai, China; <sup>2</sup>Department of Radiology, Molecular Imaging Program at Stanford (MIPS), Cancer Center, Bio-X Program, Stanford University, Stanford, California; and <sup>3</sup>Department of Bioengineering, Cancer Center, Bio-X Program, Stanford University, Stanford, California

Recently, a truncated form of the agouti-related protein (AgRP), a 4-kDa cystine-knot peptide of human origin, was used as a scaffold to engineer mutants that bound to  $\alpha_v\beta_3$  integrin with high affinity and specificity. In this study, we evaluated the potential of engineered integrin-binding AgRP peptides for use as cancer imaging agents in living subjects. **Methods:** Engineered AgRP peptides were prepared by solid-phase peptide synthesis and were folded in vitro and purified by reversed-phase high-performance liquid chromatography. Competition assays were used to measure the relative binding affinities of engineered AgRP peptides for integrin receptors expressed on the surface of U87MG glioblastoma cells. The highest-affinity mutant, AgRP clone 7C, was site-specifically conjugated with 1,4,7,10-tetraazacyclododecane-*N,N',N''N'''*-tetraacetic acid (DOTA). The resulting bioconjugate, DOTA-AgRP-7C, was radiolabeled with  $^{64}\text{Cu}$  for biodistribution analysis and small-animal PET studies in mice bearing U87MG tumor xenografts. In addition to serum stability, the in vivo metabolic stability of  $^{64}\text{Cu}$ -DOTA-AgRP-7C was assessed after injection and probe recovery from mouse kidney, liver, tumor, and urine. **Results:** AgRP-7C and DOTA-AgRP-7C bound with high affinity to integrin receptors expressed on U87MG cells (half maximal inhibitory concentration values,  $20 \pm 4$  and  $14 \pm 2$  nM, respectively). DOTA-AgRP-7C was labeled with  $^{64}\text{Cu}$  with high radiochemical purity ( $>99\%$ ). In biodistribution and small-animal PET studies,  $^{64}\text{Cu}$ -DOTA-AgRP-7C displayed rapid blood clearance, good tumor uptake and retention ( $2.70 \pm 0.93$  percentage injected dose per gram [%ID/g] and  $2.37 \pm 1.04$  %ID/g at 2 and 24 h, respectively), and high tumor-to-background tissue ratios. The integrin-binding specificity of  $^{64}\text{Cu}$ -DOTA-AgRP-7C was confirmed in vitro and in vivo by showing that a large molar excess of the unlabeled peptidomimetic c(RGDyK) could block probe binding and tumor uptake. Serum stability and in vivo metabolite assays demonstrated that engineered AgRP peptides are sufficiently stable for in vivo molec-

ular imaging applications. **Conclusion:** A radiolabeled version of the engineered AgRP peptide 7C showed promise as a PET agent for tumors that express the  $\alpha_v\beta_3$  integrin. Collectively, these results validate AgRP-based cystine-knot peptides for use in vivo as molecular imaging agents and provide support for the general use of AgRP as a scaffold to develop targeting peptides, and hence diagnostics, against other tumor receptors.

**Key Words:** cystine-knot; agouti-related protein (AgRP);  $\alpha_v\beta_3$  integrin; PET;  $^{64}\text{Cu}$

**J Nucl Med 2010; 51:251–258**

DOI: 10.2967/jnumed.109.069831

**M**olecular imaging is a rapidly growing field that has great potential to pioneer substantial improvements in the way cancer is diagnosed, staged, and ultimately treated (1–3). However, the development of imaging probes that target clinically relevant cancer biomarkers has not kept pace with the technologic capabilities of multimodality molecular imaging. To address these needs, we and others are exploring new strategies for developing imaging probes that are based on highly structured protein scaffolds, or molecular frameworks, that can be engineered to bind a myriad of diverse cancer targets.

Several characteristics are desirable when developing an engineered protein for use as a cancer imaging agent: it must bind with high affinity to a target receptor that is found predominantly on cancer cells and not on normal tissue, be specific for its target and not bind related receptors, be stable enough in serum to rapidly reach the tumor in an intact state, and be cleared by the circulation relatively quickly so that background signal is minimized (4). Many directed evolution technology platforms, together with rational methods, have been used to engineer proteins with such desired properties (5–8). As a result, novel proteins have been generated that possess high affinity and specificity for a variety of molecular targets with relevance to human disease (9–13). A common feature of these proteins is that they are relatively small and highly structured, which generally leads to fast in vivo

Received Aug. 25, 2009; revision accepted Oct. 22, 2009.

For correspondence or reprints contact either of the following:

Zhen Cheng, PhD, Department of Radiology, Molecular Imaging Program at Stanford, Cancer Center and Bio-X Program, 1201 Welch Rd., Lucas Expansion, P020A, Stanford University, Stanford, CA 94305.

E-mail: zcheng@stanford.edu

Jennifer R. Cochran, PhD, Department of Bioengineering, Cancer Center, Bio-X Program, 318 Campus Dr. West, MC 5439, James H. Clark Center, W250, Stanford University, Stanford, CA 94305-5439.

E-mail: jennifer.cochran@stanford.edu

\*Contributed equally to this work.

COPYRIGHT © 2010 by the Society of Nuclear Medicine, Inc.

clearance, rapid tumor accumulation, and sufficient in vivo stability. Optimally, these tumor-targeting proteins can be recombinantly expressed or chemically synthesized in high yield and are often modified with different molecular labels for multimodal imaging applications.

One particular class of polypeptides that offers significant promise for in vivo tumor imaging are cystine-knot mini-proteins (also known as knottins), which are characterized by a stable core motif formed by at least 3 disulfide bonds that are interwoven into a knotted conformation (14–16). This structural hallmark confers high thermal and proteolytic stability, making knottins ideal for in vivo application, for which their small size is also expected to confer rapid in vivo clearance. Recently, directed evolution has been used to validate knottins as promising scaffolds for protein engineering, through the development of novel miniproteins that effectively bind cancer targets with high affinity and specificity (17–19). In an example, a truncated form of the agouti-related protein (AgRP), a 4-kDa cystine-knot peptide with 4 disulfide bonds and 4 solvent-exposed loops (20), was successfully engineered to bind to a well-established neo-vascular tumor biomarker,  $\alpha_v\beta_3$  integrin, with single-digit nanomolar affinities (18). In another study, a 6-amino acid-constrained AgRP loop that naturally binds to the melanocortin receptor was replaced with a 9-amino acid loop that contained an integrin-binding Arg-Gly-Asp (RGD) motif. A library of 5 million AgRP mutants was randomly generated through saturation mutagenesis of the RGD-flanking residues, and each variant was expressed on the surface of an individual yeast cell as a fusion to the agglutinin mating protein, in a process known as yeast-surface display (8). The yeast-displayed AgRP library was then screened in a high-throughput manner against  $\alpha_v\beta_3$  integrin using fluorescence-activated cell sorting, to isolate mutants with high affinity and specificity for  $\alpha_v\beta_3$  integrin (18).

Here, the goals of our study were to evaluate the feasibility of using engineered AgRP peptides for developing a molecular imaging probe and increase our understanding of how cystine-knot scaffolds perform as molecular imaging probes in living subjects.

## MATERIALS AND METHODS

### General

All 9-fluorenylmethyloxycarbonyl (Fmoc)-protected amino acids were purchased from either Novabiochem/EMD Chemicals Inc. or CS Bio. The U87MG human glioblastoma cell line was obtained from the American Type Culture Collection.  $^{125}\text{I}$ -labeled echistatin and c(RGDyK) were purchased from GE Healthcare Life Sciences and Peptides International, respectively. Phosphate-buffered saline (PBS) was from Gibco/Invitrogen. All other chemicals were purchased from Fisher Scientific unless otherwise specified.

### Peptide Synthesis and Folding

AgRP linear peptide sequences were synthesized on a CS Bio CS336 instrument using Fmoc-based solid-phase peptide synthesis. Briefly, Rink Amide Resin EMD Chemicals was swollen in

*N,N*-dimethylformamide (DMF) for 30 min. Fmoc groups were removed with 20% piperidine in DMF. Aliquots of amino acids (1 mmol) were activated in a solution containing hydroxybenzotriazole (1 mmol) and diisopropylcarbodiimide (0.5 M) in DMF. After synthesis, side-chain deprotection and resin cleavage were achieved by the addition of a 94:2.5:2.5:1 (v/v) mixture of trifluoroacetic acid (TFA):triisopropylsilane:ethanedithiol:water for 2 h at room temperature. The crude product was precipitated with cold anhydrous diethyl ether and purified by reversed-phase high-performance liquid chromatography (HPLC) using a Varian Prostar instrument and Vydac  $\text{C}_{18}$  columns. Linear gradients of 90% acetonitrile in water containing 0.1% (v/v) TFA were used for all peptide purifications, which were monitored at an absorbance of 220 nm. Peptide purity was analyzed by analytical-scale reversed-phase HPLC using a Vydac  $\text{C}_{18}$  column. Molecular masses were determined by matrix-assisted laser desorption/ionization time-of-flight mass spectrometry (MALDI-TOF-MS) on a Perseptive Voyager-DE-RP Biospectrometry instrument. AgRP folding reactions were performed by incubating peptides with 4 M guanidine, 10 mM reduced glutathione, 2 mM oxidized glutathione, and 0.5 M dimethyl sulfoxide at pH 7.5. Folded peptides were purified by reversed-phase HPLC, in which they appeared as a single peak with a shorter retention times than unfolded or misfolded precursors. After purification, folded peptides were lyophilized and stored at room temperature until used. Purified peptides were dissolved in water, and concentrations were determined by amino acid analysis (AAA Service Laboratory). Peptide purity and molecular masses were determined by analytical-scale reversed-phase HPLC and MALDI-TOF-MS, respectively.

### DOTA Conjugation and $^{64}\text{Cu}$ Radiolabeling

DOTA, 1-ethyl-3-[3-(dimethylamino)propyl]carbodiimide, and *N*-hydroxysulfonosuccinimide at a molar ratio of 1:1:0.8 were mixed in water and incubated at 4°C for 30 min (pH 5.5). AgRP-7C was then added to the in situ-prepared sulfosuccinimidyl ester of DOTA in a theoretic stoichiometry of 1:5 in sodium phosphate buffer (pH 8.5–9.0). The solution was reacted at 4°C overnight, and the resulting DOTA-AgRP-7C conjugate was purified by reversed-phase HPLC and characterized by MALDI-TOF-MS as described above. DOTA-AgRP-7C (25  $\mu\text{g}$ ) was radiolabeled with  $^{64}\text{Cu}$  by the addition of 37 MBq (1 mCi) of  $^{64}\text{CuCl}_2$  (University of Wisconsin) in 0.1N sodium acetate (pH 5.5), followed by a 1-h incubation at 37°C. The radiolabeled complex was purified by a PD-10 column (GE Healthcare Life Sciences) and eluted with PBS.

### In Vitro Serum Stability

$^{64}\text{Cu}$ -DOTA-AgRP-7C (1.85–7.4 MBq [50–200  $\mu\text{Ci}$ ]) was incubated in 0.5 mL of mouse serum for various times (1–24 h) at 37°C. At each time point, the mixture was resuspended in 0.5 mL of DMF containing 5  $\mu\text{L}$  of Triton X-100 (Sigma-Aldrich) and centrifuged at 16,000g for 2 min. The supernatant containing greater than 95% of the radioactivity was filtered using a 0.22- $\mu\text{m}$  nylon SpinX column (Corning Inc.). Greater than 99% of the radioactivity passed through this filter. The samples were analyzed by radio-HPLC, and the percentage of intact peptide was determined by quantifying peaks corresponding to the intact peptide and to the degradation products.

### Cell Culture

U87MG cells were cultured in Dulbecco's modified Eagle's medium containing high glucose (GIBCO), which was supple-

mented with 10% fetal bovine serum and 1% penicillin–streptomycin. The cells were expanded in tissue culture dishes and kept in a humidified atmosphere of 5% CO<sub>2</sub> at 37°C. The medium was changed every other day. A confluent monolayer was detached with 0.5% trypsin–ethylenediaminetetraacetic acid and 0.01 M PBS (pH 7.4) and dissociated into a single-cell suspension for further cell culture and binding experiments.

### U87MG Cell Binding Assay

The U87MG cell binding assay was performed as previously described (21). Briefly,  $2 \times 10^5$  U87MG cells were incubated with 0.06 nM <sup>125</sup>I-labeled echistatin and varying concentrations of peptides in integrin-binding buffer (25 mM Tris [pH 7.4], 150 mM NaCl, 2 mM CaCl<sub>2</sub>, 1 mM MgCl<sub>2</sub>, 1 mM MnCl<sub>2</sub>, and 0.1% bovine serum albumin) at room temperature for 3 h. The cell-bound radioactivity remaining after washing was determined using a  $\gamma$ -counter. Half maximal inhibitory concentration (IC<sub>50</sub>) values were determined by nonlinear regression analysis using Kaleidagraph (Synergy Software) and are presented as the average of experiments performed on 3 separate days.

### U87MG Cell Uptake Assay

Cell uptake studies were performed as previously described (22). Briefly, U87MG cells were seeded at a density of  $0.15 \times 10^6$  in 24-well tissue culture plates and were allowed to attach overnight. The cells were washed 3 times with PBS and incubated with <sup>64</sup>Cu-DOTA-AgRP-7C (111 kBq [3  $\mu$ Ci]/well, in culture medium) with or without c(RGDyK) (2  $\mu$ g/well) at 37°C or 4°C for 15, 30, 60, and 120 min. Cells were then washed 3 times with chilled PBS containing 0.2% bovine serum albumin and detached by treatment with 0.5% trypsin–ethylenediaminetetraacetic acid. The cell suspensions were collected, and the resultant radioactivity was measured using a  $\gamma$ -counter (1470; PerkinElmer). Cell uptake of <sup>64</sup>Cu-DOTA-AgRP-7C was expressed as the percentage of added radioactivity. Experiments were performed twice with triplicate wells.

### In Vivo Metabolite Analysis

Nude mice bearing U87MG tumors were injected with <sup>64</sup>Cu-DOTA-AgRP-7C (11.1 MBq [300  $\mu$ Ci]) via the tail vein and were euthanized at 0.5 or 2 h after injection. Tumor, kidney, liver, and urine were removed, and organs were suspended in 99% DMF (0.5 mL) with 1% Triton X-100 and homogenized. All samples were then centrifuged at 16,000g for 2 min, and the supernatant was collected and filtered in 0.22- $\mu$ m nylon SpinX columns. The pellets were resuspended in solution A (99.9% H<sub>2</sub>O with 0.1% TFA) and centrifuged at 16,000g for 2 min. The final supernatants were collected and filtered through a 10-K NanoSep device (Pall Corp.). The radioactivity of the pellets and filtrates was measured using a  $\gamma$ -counter, and the extraction efficiency was then calculated as the radioactivity in the combined soluble fractions divided by the total radioactivity of the soluble and insoluble fractions. The filtrate was analyzed by radio-HPLC under identical conditions used for analyzing the original radiolabeled compound. Eluted fractions were collected every 30 s, and the radioactivity of each fraction was measured with a  $\gamma$ -counter and the resultant radio-HPLC chromatogram was plotted.

### Biodistribution Studies

All animal studies were performed in compliance with federal and local institutional rules for animal experimentation. Approximately  $10^7$  U87MG cells were suspended in PBS and sub-

cutaneously implanted in the left shoulders of female athymic *nu/nu* mice, which were supplied from Harlan at 4–5 wk of age. Tumors were allowed to grow to 0.5 cm (2–3 wk) before imaging experiments. For biodistribution studies, U87MG tumor-bearing mice ( $n = 3$  for each group) were injected with <sup>64</sup>Cu-DOTA-AgRP-7C (1.28–2.17 MBq [34.58–58.76  $\mu$ Ci], 0.298–0.506 nmol) via the tail vein and sacrificed at different time points from 0.5 to 24 h after injection. Tumor and normal tissues of interest were removed and weighed, and their radioactivity levels were measured with a  $\gamma$ -counter. The radioactivity uptake in the tumor and normal tissues was expressed as a percentage of the injected radioactive dose per gram of tissue (%ID/g). To test the  $\alpha_v\beta_3$  integrin-targeting specificity of <sup>64</sup>Cu-DOTA-AgRP-7C in vivo, U87MG tumor-bearing mice ( $n = 3$  for each group) were injected via the tail vein with a mixture of the probe (1.34–1.54 MBq [36.22–41.59  $\mu$ Ci], 0.312–0.359 nmol) and 330  $\mu$ g of c(RGDyK), an unlabeled integrin-binding peptidomimetic. The mice were sacrificed, and biodistribution of the radiolabeled peptide at 2 h after injection was determined.

### Small-Animal PET

PET of tumor-bearing mice was performed using a micro-PET R4 rodent-model scanner (Siemens Medical Solutions USA, Inc.). Mice bearing U87MG tumors were injected with <sup>64</sup>Cu-DOTA-AgRP-7C (1.89–2.17 MBq [51.18–58.76  $\mu$ Ci], 0.440–0.506 nmol) via the tail vein. At various times after injection (0.5, 1, 2, 4, and 24 h), the mice were anesthetized with isoflurane (5% for induction and 2% for maintenance in 100% O<sub>2</sub>) for imaging experiments. With the help of a laser beam attached to the scanner, the mice were placed in the prone position and near the center of the field of view of the scanner. Static scans at 24 h after injection (scanning time, 10 min) and at other time points (scanning time, 3 min) were obtained. For dynamic scanning, U87MG tumor-bearing mice were injected via the tail vein with approximately 3.7 MBq (100  $\mu$ Ci, 0.862 nmol) of <sup>64</sup>Cu-DOTA-AgRP-7C, and scans (10  $\times$  1, 10  $\times$  2, and 1  $\times$  5 min; total of 21 frames) were started roughly 2.5 min after probe injection and continued for 35 min. Images were reconstructed with a 2-dimensional ordered-subsets expectation maximization algorithm. The method for quantification analysis of small-animal PET images was the same as previously reported (23).

### Statistical Methods

Quantitative data were expressed as mean  $\pm$  SD. Means were compared using the Student *t* test. A 95% confidence level was chosen to determine the significance between groups, with *P* values of less than 0.05 indicating significant differences.

## RESULTS

### Chemistry and Radiochemistry

Engineered integrin-binding AgRP mutants (Table 1; Supplemental Fig. 1; supplemental materials are available online only at <http://jnm.snmjournals.org>) were prepared by solid-phase peptide synthesis, folded in vitro, and purified using reversed-phase HPLC. AgRP mutants (>95% purity) were characterized by MALDI-TOF-MS, and their molecular masses were found to be consistent with their theoretic masses (Table 1). Mutant AgRP-7C, which showed the highest  $\alpha_v\beta_3$  integrin-binding affinity, was site-specifically conjugated with DOTA at the peptide N terminus and

**TABLE 1.** Amino Acid Sequences and MS Characterization of AgRP Mutants

AgRP mutants	Amino acid sequences	Calculation/observed [M+H] <sup>+</sup>	U87MGIC <sub>50</sub> (nM)
AgRP	GCVRLHESCLGQQVPCDDPAATCYCRFFNAFCYCR	—	
AgRP-FN	GCVRLHESCLGQQVPCDDPAATCYCTGRGDSPASCYCR	4003.5/3998.0	1400 ± 700
AgRP-3F	GCVRLHESCLGQQVPCDDPAATCYQYRGDGMKHCYCR	4247.9/4246.5	900 ± 300
AgRP-6E	GCVRLHESCLGQQVPCDDPAATCYCVERGDGNRRCYCR	4214.8/4213.7	130 ± 20
AgRP-6F	GCVRLHESCLGQQVPCDDPAATCYCESRGDVRKCYCR	4201.9/4199.5	410 ± 90
AgRP-7C	GCVRLHESCLGQQVPCDDPAATCYCYGRGDNDLRCYCR	4221.8/4219.0	20 ± 4

Black lines represent disulfide bonds between Cys<sup>1</sup>-Cys<sup>4</sup>, Cys<sup>2</sup>-Cys<sup>5</sup>, Cys<sup>3</sup>-Cys<sup>8</sup>, and Cys<sup>6</sup>-Cys<sup>7</sup> in wild-type AgRP cystine-knot peptide.

purified by reversed-phase HPLC with greater than 95% purity (data not shown). DOTA-AgRP-7C was characterized by electrospray ionization–mass spectrometry, and the measured molecular mass of 4,607.0 Da was consistent with the theoretic mass of 4,607.2 Da for the neutral species. DOTA-AgRP-7C was labeled with <sup>64</sup>Cu by incubation with <sup>64</sup>CuCl<sub>2</sub> for 1 h at 37°C, which did not appear to denature the knottin peptide. <sup>64</sup>Cu-DOTA-AgRP-7C was purified by size-exclusion chromatography using a PD-10 column resulting in greater than 95% radiochemical purity and greater than 46% radiochemical yield. A modest specific activity of 4.29 MBq/nmol (0.058 Ci/μmol) of <sup>64</sup>Cu-DOTA-AgRP-7C was obtained at the end of synthesis (decay-corrected).

#### U87MG Cell Binding Assay

The relative integrin receptor–binding affinities of synthesized AgRP mutants, including AgRP-FN and AgRP clones 3F, 6E, 6F, and 7C (Table 1), were determined by competition binding of <sup>125</sup>I-echistatin to U87MG glioblastoma cells. Unlabeled echistatin, which has a reported dissociation constant of approximately 0.3 nM for α<sub>v</sub>β<sub>3</sub> integrin (24), was used as a positive control and to compare and validate binding experiments performed on different days. All the AgRP mutants inhibited the binding of <sup>125</sup>I-echistatin to integrin-expressing U87MG cells in a concentration-dependent manner (Fig. 1). IC<sub>50</sub> values (mean ± SD) are shown in Table 1. These studies showed that AgRP-7C possessed the highest integrin-binding affinity among the particular mutants tested (IC<sub>50</sub>, 23 ± 4 nM) and was, therefore, chosen for further studies in cell culture models and for molecular imaging in living subjects. DOTA was then site-specifically conjugated onto the N terminus of AgRP-7C using succinimide ester chemistry, and the resulting bioconjugate had an IC<sub>50</sub> value of 14 ± 2 nM, indicating that the addition of the DOTA group minimally affected integrin-binding affinity.

#### U87MG Cell Uptake Assay

U87MG cell binding and uptake experiments were performed with radiolabeled AgRP peptide and are summarized in Figure 2. <sup>64</sup>Cu-DOTA-AgRP-7C rapidly bound to cells within 15 min of incubation at both 37°C and 4°C and steadily increased. Within 1 h, the binding levels reach-

ed a plateau, and values of approximately 4.6% and approximately 2.3% of the total added radioactivity were measured for experiments conducted at 37°C and 4°C, respectively. An approximately 2-fold greater accumulation of <sup>64</sup>Cu-DOTA-AgRP-7C was observed at all time points at 37°C than with incubation at 4°C, indicating internalization that occurs at physiologic temperature. Finally, cell surface receptor binding and internalization of the radiolabeled probe were shown to be inhibited by the presence of a large molar excess of unlabeled c(RGDyK), an integrin-binding peptidomimetic. Cellular binding uptake of <sup>64</sup>Cu-DOTA-AgRP-7C at 1 h was inhibited 80% and 84% at 37°C and 4°C, respectively, in the presence of c(RGDyK), indicating that the probe was specifically targeting integrin receptors.

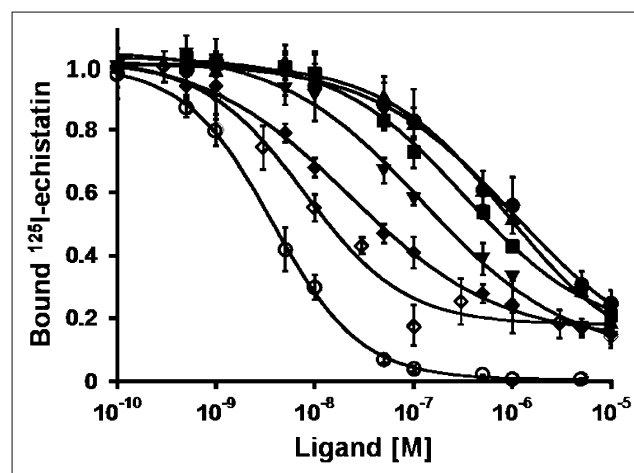


**FIGURE 1.** U87MG competition binding assay. Varying concentrations of unlabeled AgRP peptides were incubated with <sup>125</sup>I-echistatin and allowed to compete for binding to integrin receptors expressed on surface of U87MG glioblastoma cells. Fraction of <sup>125</sup>I-echistatin bound to cell surface is plotted vs. concentration of unlabeled AgRP-FN (●, 1,400 ± 700 nM), AgRP-3F (▲, 900 ± 300 nM), AgRP-6E (▼, 130 ± 20 nM), AgRP-6F (■, 410 ± 90 nM), AgRP-7C (◆, 20 ± 4 nM), DOTA-AgRP-7C (◇, 14 ± 2 nM), and echistatin (○, 3.3 ± 0.6 nM). IC<sub>50</sub> values are reported for each peptide in parentheses. Data represent mean values of binding experiments performed on 3 separate days, and error bars represent SD.

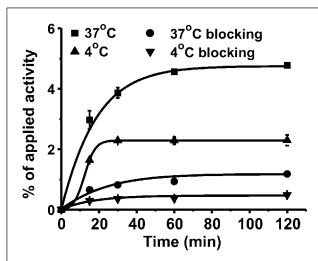


**FIGURE 2.** In vitro cell binding and uptake assay. U87MG cells were incubated with 111 kBq (3  $\mu$ Ci) of  $^{64}\text{Cu}$ -DOTA-AgRP-7C for various time points at 4°C or 37°C, with or without addition of 2  $\mu$ g of c(RGDyK) integrin-binding peptide. Data represents mean percentage of total radioactivity added, measured in triplicate, and error bars represent SD.

### In Vitro Stability and Metabolite Analysis

To test serum stability, 5  $\mu$ L of purified  $^{64}\text{Cu}$ -DOTA-AgRP-7C were incubated in 200  $\mu$ L of mouse serum at 37°C, and radio-HPLC analysis indicated that approximately 80% of the probe remained intact after 24 h (Supplemental Fig. 2). Next, the metabolic fate of  $^{64}\text{Cu}$ -DOTA-AgRP-7C was determined from samples recovered from the tumor, liver, kidney, and urine of human tumor xenograft models. The probe was injected into U87MG tumor-bearing mice via the tail vein, and the various tissues were homogenized at 0.5 and 2 h after injection. The efficiency of probe extraction from homogenized tissues was 60%–80% (Table 2). In tumor tissues, 70% and 16% of the probe remained intact at 0.5 and 2 h after injection, respectively (Supplemental Fig. 2). For the same time points, approximately 62% and 16% of the probe was intact from the liver and 83% and 19% of the probe was intact from the kidneys (Supplemental Fig. 2). Finally, the probe was recovered essentially intact from urine samples obtained up to 2 h after injection (Supplemental Fig. 2).

### Biodistribution Studies

The in vivo biodistribution of  $^{64}\text{Cu}$ -DOTA-AgRP-7C in mice bearing U87MG tumors was determined at various times after injection (Table 3). Rapid accumulation of the probe in the tumor was observed at early time points ( $1.92 \pm 0.48$  %ID/g at 0.5 h after injection). At later time points, tumor uptake increased and reached  $2.70 \pm 0.93$  and  $2.37 \pm 1.04$  %ID/g at 2 and 24 h, respectively, after injection.  $^{64}\text{Cu}$ -DOTA-AgRP-7C displayed rapid blood

**TABLE 2.** Serum Stability and In Vivo Metabolite Analysis Data of  $^{64}\text{Cu}$ -DOTA-AgRP-7C

Tissue	Time (h)	Stability (%)	Extraction efficiency (%)
Urine	0.5	95	100
	2	88	100
Tumor	0.5	70	57
	2	16	64
Liver	0.5	62	58
	2	16	60
Kidney	0.5	83	81
	2	19	80
Serum	24	81	95

clearance, as determined by the radioactivity remaining in the blood at 0.5 h after injection ( $0.70 \pm 0.07$  %ID/g). Moreover,  $^{64}\text{Cu}$ -DOTA-AgRP-7C showed low muscle uptake of  $0.27 \pm 0.03$  %ID/g at 0.5 h after injection, which decreased to  $0.12 \pm 0.01$  %ID/g at 24 h after injection. Accumulation of the probe in the liver was also low, with values of  $1.09 \pm 0.13$  %ID/g at 0.5 h and  $2.04 \pm 0.34$  %ID/g at 24 h. In contrast, high probe uptake was observed in the kidneys, with a value of  $31.08 \pm 13.52$  %ID/g observed at 0.5 h after injection, which increased 2–4 h after injection but decreased to 24.04 %ID/g at 24 h after injection (Table 3). These data clearly indicate that the probe is excreted and metabolized by the kidneys and not the liver.

$^{64}\text{Cu}$ -DOTA-AgRP-7C displayed high tumor-to-background tissue (blood, muscle, lung, liver, spleen, and pancreas) ratios (Table 4), which bodes well for their application as in vivo molecular imaging agents. For example, at 4 h after injection, the tumor-to-blood and tumor-to-muscle ratios of  $^{64}\text{Cu}$ -DOTA-AgRP-7C were  $20.87 \pm 1.42$  and  $11.32 \pm 1.17$ , respectively. Moreover, with the rapid clearance of the probe from nontarget tissues, several of the tumor-to-background tissue ratios increased with time from 0.5 to 4 h (Table 4).

The  $\alpha_v\beta_3$  integrin-binding specificity of  $^{64}\text{Cu}$ -DOTA-AgRP-7C to receptors was evaluated in vivo by the coinjection of a large molar excess of unlabeled c(RGDyK), which competes for or blocks radioligand binding (Table 3). Coinjection with c(RGDyK), compared with injection of the probe alone, significantly reduced the tumor uptake of  $^{64}\text{Cu}$ -DOTA-AgRP-7C by approximately 64% ( $0.98 \pm 0.18$  vs.  $2.70 \pm 0.93$  %ID/g at 2 h after injection;  $P < 0.05$ ). In contrast, there was no significant difference observed in nontarget tissues between mice that were injected with  $^{64}\text{Cu}$ -DOTA-AgRP-7C, with or without coinjection of c(RGDyK).

### Small-Animal PET

Representative coronal and transverse small-animal PET images of U87MG tumor-bearing mice ( $n = 3$ ) at different time points (0.5, 1, 2, 4, and 24 h) after injection are shown in Figure 3. The tumors were clearly visible at 0.5 h after injection and demonstrated high contrast with low contralateral background from 0.5 to 4 h, which persisted to 24 h after injection. High kidney uptake was observed at early time points and beyond, again indicating a renal clearance route. Most of the nontarget organs demonstrated relatively low accumulation of the probe. Small-animal PET image analysis of tumors and major organs was performed by measuring the signal intensities corresponding to regions of interest that encompassed the entire organ represented by coronal image slices (Fig. 3). The small-animal PET quantification results, in general, agreed well with the biodistribution data; however, the small-animal PET data for kidneys was lower, as might be partly due to the detector dead-time losses, interdetector gaps, and block detector effects.

The pharmacokinetic and tumor-targeting properties of  $^{64}\text{Cu}$ -DOTA-AgRP-7C in a U87MG tumor-bearing mouse were evaluated with a 35-min dynamic small-animal PET

**TABLE 3.** Biodistribution Results for <sup>64</sup>Cu-DOTA-AgRP-7C in Nude Mice Bearing Subcutaneously Xenotransplanted U87MG Human Glioblastoma

Organ	%ID/g <sup>64</sup> Cu-DOTA-AgRP-7C				<sup>64</sup> Cu-DOTA-AgRP-7C + c(RGDyK) at 2 h
	0.5 h	2 h	4 h	24 h	
Tumor	1.92 ± 0.48	2.70 ± 0.93	1.9 ± 0.35	2.37 ± 1.04	0.98 ± 0.18*
Blood	0.70 ± 0.07	0.41 ± 0.14	0.09 ± 0.02	0.23 ± 0.01	0.33 ± 0.11
Heart	0.37 ± 0.07	0.37 ± 0.03	0.19 ± 0.06	0.5 ± 0.06	0.29 ± 0.06
Liver	1.09 ± 0.13	1.74 ± 0.72	1.67 ± 0.35	2.04 ± 0.34	1.94 ± 0.24
Lungs	1.17 ± 0.04	1.18 ± 0.23	0.51 ± 0.11	1.16 ± 0.20	0.79 ± 0.13
Muscle	0.27 ± 0.03	0.14 ± 0.01	0.17 ± 0.02	0.12 ± 0.01	0.49 ± 0.29
Kidney	31.08 ± 13.52	60.22 ± 17.52	56.03 ± 1.93	24.04 ± 7.53	67.73 ± 3.65
Spleen	0.83 ± 0.05	1.17 ± 0.17	0.81 ± 0.17	0.64 ± 0.04	0.69 ± 0.35
Brain	0.05 ± 0.01	0.03 ± 0.01	0.04 ± 0.01	0.07 ± 0.01	0.04 ± 0.02
Intestine	1.4 ± 0.25	1.37 ± 0.24	0.67 ± 0.12	1.2 ± 0.19	1.03 ± 0.20
Skin	0.99 ± 0.07	0.73 ± 0.09	0.5 ± 0.08	0.47 ± 0.09	0.44 ± 0.35
Stomach	1.81 ± 0.09	1.42 ± 0.38	0.61 ± 0.10	1.01 ± 0.13	0.82 ± 0.26
Pancreas	0.26 ± 0.04	0.28 ± 0.04	0.09 ± 0.02	0.3 ± 0.02	0.68 ± 0.49
Bone	0.43 ± 0.09	1.19 ± 0.51	0.29 ± 0.07	0.59 ± 0.04	1.26 ± 0.24

\**P* < 0.05, compared with <sup>64</sup>Cu-DOTA-AgRP-7C data at 2 h. Data are presented as %ID/g tissue ± SD (*n* = 3).

Data are expressed as %ID/g after intravenous injection of probe (1.28–2.17 MBq [34.58–58.76 μCi]) at 0.5, 2, 4, and 24 h (*n* = 3). For 2-h block group, mice were coinjected with c(RGDyK).

scan. As shown in Figure 4, the probe was rapidly cleared from blood circulation as determined by region-of-interest analysis of the heart. At 35 min after injection, radioactivity levels in the heart rapidly decreased to approximately 20% of the dose recorded during the first 30 s of the scan. In contrast, tumor uptake gradually increased with time from 1.46 %ID/g at 1 min to 3.79 %ID/g at 35 min after injection. Low levels of liver and muscle uptake were observed (Fig. 4). Most of the probe was excreted through the kidneys almost immediately on injection and led to high signals throughout the experiment, consistent with the results observed in the biodistribution studies.

## DISCUSSION

Cystine-knot peptides are emerging as promising scaffolds for the development of affinity ligands that bind to cancer biomarkers. Recently, several cystine-knot peptides, including the *Ecballium elaterium* trypsin inhibitor (EETI-II) and AgRP, have been used as scaffolds to engineer peptides that

bind integrin receptors with low nanomolar affinities (17,18). EETI-II- and AgRP-based cystine peptides are small (3–4 kDa), are amenable to amino acid substitutions, and have high chemical, thermal, and proteolytic stability (25,26). As a result, they were able to survive both exposure to serum proteases and the reaction conditions required for radiometal conjugation in our studies.

In this study, for the first time to our knowledge, the potential of a radiolabeled engineered integrin-binding AgRP peptide for use as a cancer molecular imaging agent was evaluated in human tumor xenograft models. Using in vivo biodistribution data and small-animal PET data, we showed that <sup>64</sup>Cu-DOTA-AgRP-7C had favorable tumor-targeting properties including rapid and high tumor uptake, rapid clearance from blood and most normal tissues, and high tumor-to-normal tissue ratios. In our previous study, the EETI-II-based integrin-binding PET probes <sup>64</sup>Cu-DOTA-EETI-2.5D and <sup>64</sup>Cu-DOTA-EETI-2.5F both showed excellent in vivo tumor-targeting properties but exhibited much lower levels of kidney uptake and retention (5–10 %ID/g)

**TABLE 4.** Tumor-to-Normal Tissue Ratios for <sup>64</sup>Cu-DOTA-AgRP-7C in Nude Mice Bearing U87MG Xenografts

Ratio	<sup>64</sup> Cu-DOTA-AgRP-7C				<sup>64</sup> Cu-DOTA-AgRP-7C + c(RGDyK) at 2 h
	0.5 h	2 h	4 h	24 h	
Tumor-to-blood	2.77 ± 0.86	6.59 ± 1.19	20.87 ± 1.42	10.3 ± 4.34	3.10 ± 0.61*
Tumor-to-muscle	7.28 ± 2.51	17.17 ± 4.59	11.32 ± 1.17	18.82 ± 7.17	2.53 ± 1.39*
Tumor-to-liver	1.79 ± 0.57	1.73 ± 1.38	1.15 ± 0.05	1.13 ± 0.37	0.52 ± 0.16
Tumor-to-lung	1.63 ± 0.37	1.99 ± 0.36	3.71 ± 0.09	1.98 ± 0.60	1.24 ± 0.06*
Tumor-to-spleen	2.30 ± 0.55	2.04 ± 0.60	2.48 ± 0.98	3.63 ± 1.44	1.68 ± 0.85
Tumor-to-pancreas	7.47 ± 1.62	7.95 ± 5.12	21.81 ± 6.74	5.53 ± 3.22	1.96 ± 1.44*
Tumor-to-kidneys	0.07 ± 0.04	0.04 ± 0.03	0.03 ± 0.01	0.08 ± 0.06	0.01 ± 0.00

\**P* < 0.05, compared with <sup>64</sup>Cu-DOTA-AgRP-7C data at 2 h. Data are presented as mean ± SD (*n* = 3).

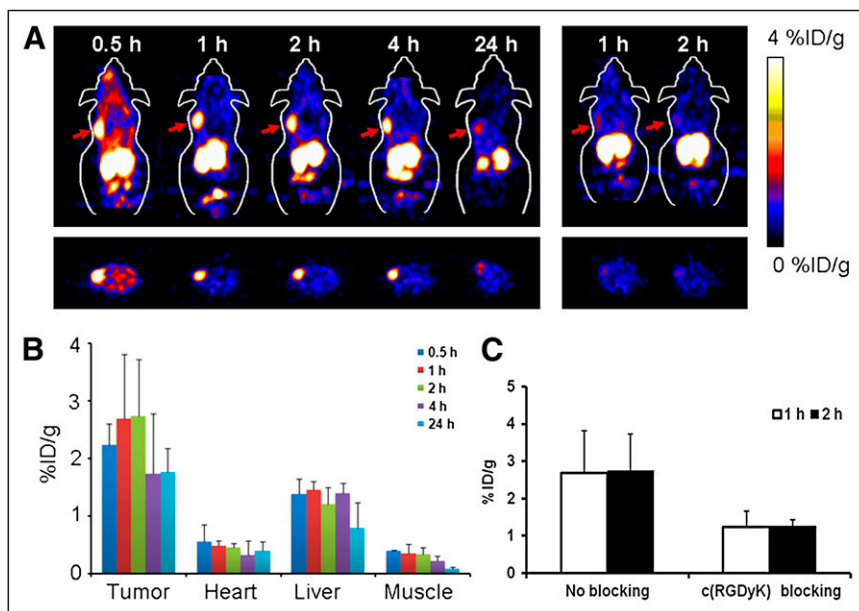


**FIGURE 3.** Small-animal PET and quantification. (A) Representative coronal and transverse small-animal PET images of U87MG tumor-bearing mice at 0.5, 1, 2, 4, and 24 h after injection of 2.22 MBq ( $\approx 60 \mu\text{Ci}$ ) of  $^{64}\text{Cu}$ -DOTA-AgRP-7C. Small-animal PET images acquired at 1 and 2 h after coinjection of 330  $\mu\text{g}$  of c(RGDyK) (right). (B) Quantification analysis of radioactivity accumulation in selected organs at different time points after injection of  $^{64}\text{Cu}$ -DOTA-AgRP-7C, reported as %ID/g. (C) Quantification analysis of radioactivity accumulation of probe in tumor with or without coinjection of c(RGDyK) at 1 and 2 h after injection.

than  $^{64}\text{Cu}$ -DOTA-AgRP-7C (30–60 %ID/g) (19). The rapid systemic clearance and high kidney uptake of  $^{64}\text{Cu}$ -DOTA-AgRP-7C may also quickly deplete circulating tracer concentrations and thus may lead to the lower tumor uptake values reported here than those for  $^{64}\text{Cu}$ -DOTA-EETI-2.5D and  $^{64}\text{Cu}$ -DOTA-EETI-2.5F, which accumulate in the tumor at approximately 2–4 %ID/g higher at the same time points (19). However, high tumor-to-normal tissue ratios were achieved for both EETI-II-based and AgRP-based integrin-binding peptides, indicating that both of these cystine-knot scaffolds show promise in molecular imaging applications related to cancer.

The tertiary structures across cystine-knot-containing peptides are conceptually similar in that they contain a stabilized disulfide-bonded core, which forms the basis for several surface-exposed loops that differ vastly in primary structure (14). These loop regions appear to influence the overall stability, as comparisons between the stability of wild-type AgRP and EETI-II on exposure to gastric proteases have shown (27). In general, our results agree with these previous studies in that EETI-II-based peptides are much more stable in vivo than AgRP-based peptides. Although their serum stability appears to be similar,  $^{64}\text{Cu}$ -DOTA-EETI-2.5D remains 80% intact in tumor tissue at 4 h after

injection (19), compared with  $^{64}\text{Cu}$ -DOTA-AgRP-7C, which is essentially degraded after 2 h. Probe behavior observed in normal tissues also reflected these trends. Interestingly, only intact  $^{64}\text{Cu}$ -DOTA-AgRP-7C was recovered from the urine and blood serum. Collectively, these results suggest that the probe is stable in the bloodstream, and once broken down in other parts of the body the resulting metabolites accumulate and are retained in the kidneys and are not excreted in the waste. However, it is also possible that the fragments we observed by radio-HPLC are due to the release of uncoordinated  $^{64}\text{Cu}$  from radiolabeled peptide facilitated by transchelation with enzymes residing in the tumor and other organs (28) and do not represent a breakdown of the cystine-knot peptide.

Further optimization of the AgRP-based probe to achieve improved tumor-targeting properties is a goal we are actively pursuing. The use of different radioisotopes, such as radio-halogens, or the addition of various linkers and prosthetic groups, such as glycosyls or high-molecular-weight polyethyleneglycol molecules, may lead to improvement in tracer pharmacokinetics and tumor-targeting ability (29,30). In the literature, several strategies have been successful in reducing kidney uptake of radiolabeled peptides. These strategies include coinjection of cations such as lysine or polylysine

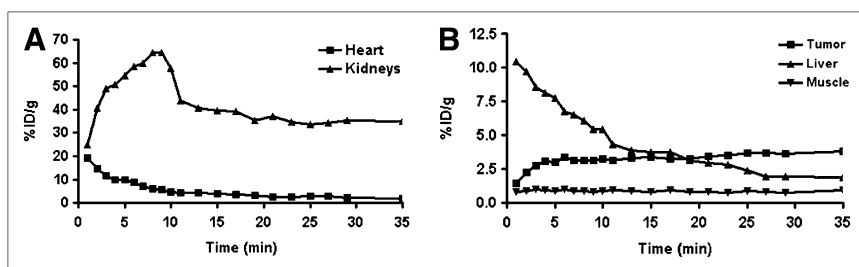


**FIGURE 4.** Dynamic small-animal PET scans. Time-activity plots of major organs in a U87MG tumor-bearing mouse after intravenous injection of  $\approx 3.7$  MBq ( $\approx 100 \mu\text{Ci}$ ) of  $^{64}\text{Cu}$ -DOTA-AgRP-7C.

(22,31). Finally, there is a growing body of evidence that shows that  $\alpha_v\beta_3$  integrin is highly correlated to the invasiveness and metastasis of many malignant human tumors. Numerous integrin imaging agents have been reported in the literature, but most research has mainly focused on using small cyclic RGD-containing peptides and their derivatives (29,30,32). Compared with the  $^{64}\text{Cu}$ -labeled monomeric DOTA-conjugated c(RGDyK), our AgRP scaffold-based probe generally shows comparable tumor uptake and relatively lower liver uptakes (19,32).

Our goal in this study was to evaluate the potential of the AgRP cystine-knot scaffold as an in vivo molecular imaging agent against a well-characterized target; in the future, we will develop affinity ligands for targets that are not readily accessible by small cyclic peptides or small molecules. The versatility and promise shown thus far by cystine-knot scaffolds is hypothesized to lead to the development of several new probes against clinically relevant targets for which affinity ligands currently do not exist.

## CONCLUSION

In this study, we evaluated the potential of the  $\alpha_v\beta_3$  integrin-binding knottin peptide  $^{64}\text{Cu}$ -DOTA-AgRP-7C for use as an imaging agent in living subjects. The AgRP variant 7C showed high integrin-binding affinity and target-binding specificity both in vitro and in vivo. As a PET probe,  $^{64}\text{Cu}$ -DOTA-AgRP-7C showed rapid tumor uptake, high tumor-to-background tissue contrast, and favorable pharmacokinetics, demonstrating its potential for  $\alpha_v\beta_3$  integrin-positive tumor imaging. Collectively, these results indicate that knottin peptides are promising scaffolds for engineering and clinical translation of new in vivo molecular imaging probes.

## ACKNOWLEDGMENTS

This work was supported in part by National Cancer Institute (NCI) 5R01 CA119053, NCI In Vivo Cellular Molecular Imaging Center (ICMIC) grant P50 CA114747, NCI 5K01 CA104706, and a Stanford Molecular Imaging Scholars postdoctoral fellowship R25 CA118681. Moreover, this work was also funded by a fellowship from China Scholarship Council, a Faculty Scholar Award from the Edward Mallinckrodt Jr. Foundation, and the Canary Foundation.

## REFERENCES

- Gambhir SS. Molecular imaging of cancer with positron emission tomography. *Nat Rev Cancer*. 2002;2:683–693.
- Massoud TF, Gambhir SS. Molecular imaging in living subjects: seeing fundamental biological processes in a new light. *Genes Dev*. 2003;17:545–580.
- Weissleder R. Molecular Imaging in Cancer. *Science*. 2006;312:1168–1171.
- Friedman M, Stahl S. Engineered affinity proteins for tumour-targeting applications. *Biotechnol Appl Biochem*. 2009;53:1–29.
- Ladner RC. Polypeptides from phage display. A superior source of in vivo imaging agents. *Q J Nucl Med*. 1999;43:119–124.

- Lipovsek D, Plückthun A. In-vitro protein evolution by ribosome display and mRNA display. *J Immunol Methods*. 2004;290:51–67.
- Uchiyama F, Tanaka Y, Minari Y, Tokui N. Designing scaffolds of peptides for phage display libraries. *J Biosci Bioeng*. 2005;99:448–456.
- Gai SA, Wittrup KD. Yeast surface display for protein engineering and characterization. *Curr Opin Struct Biol*. 2007;17:467–473.
- Binz HK, Amstutz P, Pluckthun A. Engineering novel binding proteins from nonimmunoglobulin domains. *Nat Biotechnol*. 2005;23:1257–1268.
- Hosse RJ, Rothe A, Power BE. A new generation of protein display scaffolds for molecular recognition. *Protein Sci*. 2006;15:14–27.
- Nilsson FY, Tolmachev V. Affibody molecules: new protein domains for molecular imaging and targeted tumor therapy. *Curr Opin Drug Discov Devel*. 2007;10:167–175.
- Kolmar H. Biological diversity and therapeutic potential of natural and engineered cystine knot miniproteins. *Curr Opin Pharmacol*. 2009;9:608–614.
- Gebauer M, Skerra A. Engineered protein scaffolds as next-generation antibody therapeutics. *Curr Opin Chem Biol*. 2009;13:245–255.
- Pallaghy PK, Nielsen KJ, Craik DJ, et al. A common structural motif incorporating a cystine knot and a triple-stranded  $\beta$ -sheet in toxic and inhibitory polypeptides. *Protein Sci*. 1994;3:1833–1839.
- Daly NL, Clark RJ, Craik DJ. Disulfide folding pathways of cystine-knot proteins: tying the knot within the circular backbone of the cyclotides. *J Biol Chem*. 2003;278:6314–6322.
- Kolmar H. Alternative binding proteins: biological activity and therapeutic potential of cystine-knot miniproteins. *FEBS J*. 2008;275:2684–2690.
- Kimura RH, Levin AM, Cochran FV, et al. Engineered cystine knot peptide that bind  $\alpha_v\beta_3$ ,  $\alpha_v\beta_5$ , and  $\alpha_5\beta_1$  integrins with low nanomolar affinity. *Proteins*. 2009;77:359–369.
- Silverman AP, Levin AM, Lahti JL, et al. Engineered cystine-knot peptides that bind  $\alpha_v\beta_3$  integrin with antibody-like affinities. *J Mol Biol*. 2009;385:1064–1075.
- Kimura RH, Cheng Z, Gambhir SS, et al. Engineered knottin peptides: a new class of agents for imaging integrin expression in living subjects. *Cancer Res*. 2009;69:2435–2442.
- Jackson PJ, McNulty JC, Yang YK, et al. Design, pharmacology, and NMR structure of a minimized cystine knot with agouti-related protein activity. *Biochemistry*. 2002;41:7565–7572.
- Cheng Z, Wu Y, Xiong Z, et al. Near-infrared fluorescent RGD peptides for optical imaging of integrin  $\alpha_v\beta_3$  expression in living mice. *Bioconjug Chem*. 2005;16:1433–1441.
- Cheng Z, Chen J, Quinn TP, et al. Radioiodination of rhenium cyclized  $\alpha$ -melanocyte-stimulating hormone resulting in enhanced radioactivity localization and retention in melanoma. *Cancer Res*. 2004;64:1411–1418.
- Cheng Z, Xiong Z, Subbarayan M, et al. Cu-labeled  $\alpha$ -melanocyte-stimulating hormone analog for microPET imaging of melanocortin 1 receptor expression. *Bioconjug Chem*. 2007;18:765–772.
- Kumar CC, Nie H, Rogers CP, et al. Biochemical characterization of the binding of echistatin to integrin  $\alpha_v\beta_3$  receptor. *J Pharmacol Exp Ther*. 1997;283:843–853.
- Craik DJ, Daly NL, Waine C. The cystine knot motif in toxins and implications for drug design. *Toxicon*. 2001;39:43–60.
- Chiche L, Heitz A, Gelly JC, et al. Squash inhibitors: from structural motifs to macrocyclic knottins. *Curr Protein Pept Sci*. 2004;5:341–349.
- Werle M, Schmitz T, Huang HL, et al. The potential of cystine-knot microproteins as novel pharmacophoric scaffolds in oral peptide drug delivery. *J Drug Target*. 2006;14:137–146.
- Sun X, Wuest M, Weisman GR, et al. Radiolabeling and in vivo behavior of copper-64-labeled cross-bridged cyclam ligands. *J Med Chem*. 2002;45:469–477.
- Chen X, Park R, Hou Y, et al. MicroPET imaging of brain tumor angiogenesis with  $^{18}\text{F}$ -labeled PEGylated RGD peptide. *Eur J Nucl Med Mol Imaging*. 2004;31:1081–1089.
- Wu Z, Li ZB, Cai W, et al.  $^{18}\text{F}$  labeled mini-PEG spacers RGD dimer ( $^{18}\text{F}$ -FPRGD<sub>2</sub>): synthesis and microPET imaging of  $\alpha_v\beta_3$  integrin expression. *Eur J Nucl Med Mol Imaging*. 2007;34:1823–1831.
- Chen J, Cheng Z, Hoffman TJ, et al. Melanoma-targeting properties of  $^{99\text{m}}\text{Tc}$ -labeled cyclic  $\alpha$ -melanocyte-stimulating hormone peptide analogues. *Cancer Res*. 2000;60:5649–5658.
- Chen X, Park R, Tohme M, Shahinian AH, Bading JR, Conti PS. MicroPET and autoradiographic imaging of breast cancer  $\alpha_v$ -integrin expression using  $^{18}\text{F}$ - and  $^{64}\text{Cu}$  labeled RGD peptide. *Bioconjug Chem*. 2004;15:41–49.